

## ImaGiNe Seldinger

Luboz, Vincent; Zhang, Yan; Johnson, Sheena; Song, Yi; Kilkenny, C.; Hunt, C.; Zhai, J.; Woolnough, H.; Guediri, S.; John, Nigel; Bello, F. ; Gould, Derek

*Published in:*  
Computer Methods and Programs in Biomedicine

*DOI:*  
[10.1016/j.cmpb.2013.05.014](https://doi.org/10.1016/j.cmpb.2013.05.014)

*Publication date:*  
2013

*Document Version*  
Author accepted manuscript

[Link to publication in ResearchOnline](#)

*Citation for published version (Harvard):*  
Luboz, V, Zhang, Y, Johnson, S, Song, Y, Kilkenny, C, Hunt, C, Zhai, J, Woolnough, H, Guediri, S, John, N, Bello, F & Gould, D 2013, 'ImaGiNe Seldinger: first simulator for Seldinger technique and angiography training', *Computer Methods and Programs in Biomedicine*, vol. 111, no. 2, pp. 419-434.  
<https://doi.org/10.1016/j.cmpb.2013.05.014>

### General rights

Copyright and moral rights for the publications made accessible in the public portal are retained by the authors and/or other copyright owners and it is a condition of accessing publications that users recognise and abide by the legal requirements associated with these rights.

### Take down policy

If you believe that this document breaches copyright please view our takedown policy at <https://edshare.gcu.ac.uk/id/eprint/5179> for details of how to contact us.

1  
2  
3  
4  
5  
6  
7  
8  
9 ImaGiNe Seldinger: first simulator for Seldinger technique and angiography training  
10  
11 V. Luboz, Y. Zhang, S. Johnson, Y. Song, C. Kilkenny, C. Hunt, H. Woolnough, S. Guediri, J. Zhai, T.  
12 Odetoyinbo, P. Littler, A. Fisher, C. Hughes, N. Chalmers, D. Kessel, P. J. Clough, J. Ward, R. Phillips, T.  
13 How, A. Bulpitt, N. W. John, F. Bello, D. Gould  
14  
15 Collaborators in Radiological Interventional Virtual Environments (CRaIVE)  
16  
17 (<http://www.craive.org.uk/>)  
18  
19

20 Corresponding author: Vincent Luboz, [vincent.luboz@gmail.com](mailto:vincent.luboz@gmail.com)  
21 Laboratoire TIMC-IMAG  
22 Faculte de Medecine  
23 38706 La Tronche  
24 France  
25 Telephone: +33 4 76 52 00 05  
26 Fax: +33 4 76 52 00 55  
27  
28  
29

30 **Abstract.**  
31

32 In vascular interventional radiology, procedures generally start with the Seldinger technique to access the  
33 vasculature, using a needle through which a guidewire is inserted, followed by navigation of catheters within the  
34 vessels. Visual and tactile skills are learnt in a patient apprenticeship which is expensive and risky for patients. We  
35 propose a training alternative through a new virtual simulator supporting the Seldinger technique: ImaGiNe  
36 (Imaging Guided interventional Needle) Seldinger. It is composed of two workstations: 1) a simulated pulse is  
37 palpated, in an immersive environment, to guide needle puncture, 2) two haptic devices provide a novel interface  
38 where a needle can direct a guidewire and catheter within the vessel lumen, using virtual fluoroscopy. Different  
39 complexities are provided by 28 real patient datasets. The feel of the simulation is enhanced by replicating, with the  
40 haptics, real force and flexibility measurements. A preliminary validation study has demonstrated training  
41 effectiveness for skills transfer.  
42  
43  
44  
45  
46  
47  
48  
49  
50  
51

52 **Keywords:** Interventional radiology, Vascular surgery, Seldinger technique, Training, Virtual simulation, Haptics  
53 devices.  
54  
55  
56  
57  
58  
59  
60  
61  
62  
63  
64  
65

## 1. Introduction

Vascular interventional radiology techniques consist of inserting and navigating anatomically configured, soft tipped wires and catheters within the vascular tree, using X-ray fluoroscopy for visualization. These techniques enable a range of pathologies (e.g. bleeding, tumour, arterial blockage, aneurysms) to be treated, and represent an effective alternative to open surgery. Nevertheless, gaining access to the vessels and navigating instruments within them, requires skills that are difficult to train and acquire. Percutaneous access to an artery or vein relies on the Seldinger technique (Seldinger, 1953), where a needle is guided by the operator's sense of touch, or ultrasound imaging. In the classical method of arterial puncture, an operator uses anatomical bone landmarks and arterial pulsations to guide correct needle placement within the arterial lumen. Most frequently this is the common femoral artery. When a jet of arterial blood is demonstrated, a guidewire is carefully introduced through the needle into the vessel lumen, using tactile sensations to avoid complications due to misdirection of the wire. Once sufficient guidewire has been advanced into the vessel, the needle is removed and a catheter is inserted over the wire, into the vessel. The combination of wire and catheter, visualised using X-ray fluoroscopy, can then be navigated using rotation and translation actions by the operator.

Such manipulations are frequently carried out within diseased vessels, where avoiding complications such as vessel perforation, whilst attaining a satisfactory therapeutic result, requires the clinician's careful attention to fluoroscopy imaging and his/her sense of touch. Hence, successful outcomes rely on high levels of core, psychomotor skills, which are trained in an apprenticeship that provides repeated, varied practice of interventions in patients. Despite expert supervision, there is an inevitable risk from the operator's lack of expertise that may lead to patient discomfort, pain and even complications. Only when proficiency at a given level is attained, can the trainee progress to more complex cases. This training model is clearly limited, not only by the available cases and the time taken for teaching, but also by the advent of working time directives, patients' perceptions of risk, and the availability of an expert mentor. Several alternative training methods have been proposed to overcome these limitations. Using a silicon rubber vascular phantom avoids any risk for the patient, but leads to a biased sense of touch since silicon elasticity and friction is dissimilar to that of soft tissues and vessel walls. Training on cadavers or animals is expensive, and lacks realistic blood flow and other physiology in the former, while presenting significant anatomical differences in the latter.

1  
2  
3  
4  
5  
6  
7  
8  
9 A further method uses computer based simulations based on virtual human anatomies, where vessel and tissue  
10 elasticity, as well as instrument behaviour can potentially be modelled closely. This technology brings the added  
11 benefit of accurately evaluating trainee performance within a risk free environment, without limit on the duration  
12 and frequency of training. Several commercial virtual simulators have been validated for training procedural skills in  
13 laparoscopic surgery, endotracheal intubation and colonoscopy (Seymour et al., 2002, Rowe and Cohen, 2002).  
14 Such evidence has been slower to accrue for vascular IR training simulators, particularly for the training of core  
15 skills (Chaer et al., 2006). These commercial vascular IR virtual environments offer a range of scenarios and  
16 pathologies, as well as an extensive range of instruments. However, there is a lack of fidelity for fine and critical  
17 navigational manipulations of the virtual instruments, questioning their potential to transfer these fine motor skills to  
18 procedures performed in patients. Moreover, there is limited accuracy for modelling vascular anatomy, pathology,  
19 deformation and physiology, which are key properties of real vessel behaviour. Finally, no existing simulator allows  
20 Seldinger technique training, despite the challenge it represents for non experienced clinicians.  
21  
22 Research studies have been conducted to improve the basic skills training of vascular IR, either for needle puncture  
23 or for navigation of the instruments within vessels. Traditional needle puncture simulators use real needles and  
24 mannequins with multiple tissue layers representing epidermis, dermis, fat layer, muscle layer, etc. Tissue layers are  
25 generally changeable. Some haptics feedback is provided to the learner by the pre-set tissue resistance. A review of  
26 such haptics feedback is given in (Coles et al., 2011). Examples of this kind of simulators include the advanced  
27 Venipuncture Arm from Limbs & Things (<http://golimbs.com>), the Epidural Injection Simulator® from Flinders  
28 MediTech (<http://flindersmeditech.com>), and the Life/form® Spinal Injection Simulator from Enasco  
29 (<http://www.enasco.com>). Advanced researches in needle puncture simulators make use of commercial force/torque  
30 hardware to provide force feedback. Some haptics needle puncture simulators connect a haptics device to a fixed  
31 insertion point on a mannequin. For example, The Mediseus Epidural simulator (Medic Vision) (Mayooran et al.,  
32 2006) uses a Sensable PHANToM Omni with a modified syringe end effector; the EpiSim  
33 (<http://www.yantric.com>), originally developed by MIT (Dang et al., 2001), also utilizes a PHANToM haptics  
34 device to simulate a spinal injection. Some simulators use haptics devices to operate virtual needles and no physical  
35 mannequins are involved. For example, the ultrasound-guided needle puncture simulation implemented by Vidal et  
36 al (2008) uses two PHANToM Omni devices and employs an immersive workbench. One of the first vascular IR  
37 simulators for instrument navigation used finite element methods (FEM) to model the interaction between the  
38  
39  
40  
41  
42  
43  
44  
45  
46  
47  
48  
49  
50  
51  
52  
53  
54  
55  
56  
57  
58  
59  
60  
61  
62  
63  
64  
65

1  
2  
3  
4  
5  
6  
7  
8  
9 surgical instruments and vasculature (Chui et al., 2002). The instruments were modelled as a system of flexible  
10 multiple bodies. The Simulation Group at CIMIT developed a suite of simulation tools for IR, including an accurate  
11 catheter simulation system (Cotin et al., 2005) interacting with a 3D vasculature and integrating flow simulation.  
12  
13 The instruments are modelled as non-linear deformable beam elements, while blood flow is simulated via a  
14 volumetric approach. The Image Sciences Institute of Utrecht uses Cosserat models to model a guidewire as a set of  
15 straight, non-bendable, incompressible beams with perfect torque control (Alderliesten et al., 2007). Such models  
16 consider two types of energy (bending and external contact) and are more accurate and efficient than spring meshes  
17 or 3D FEM meshes for thin solids, but real-time simulation is hard to achieve.  
18  
19 The CRAIVE consortium (Collaborators in Radiological Interventional Virtual Environments, - [www.craive.org.uk](http://www.craive.org.uk))  
20 has been developing its own virtual environment since 2006. Its ImaGiNe Seldinger simulator aims at training the  
21 Seldinger technique and navigation of instruments within vessels. The main contribution of this work is the  
22 simulator as a whole, with its unique capability to train Seldinger access and catheterization. The novelties concern  
23 the simulator design, the use of force data readings from patients, the sensors developed specially for the task (in  
24 particular a patented haptic needle holder), and the metrics used to analyse the trainee's performance. Because of  
25 current hardware limitations, ImaGiNe Seldinger is divided into two workstations: a needle puncture simulator and a  
26 catheterisation simulator. These two workstations are presented in sections 2.2 and 2.3 after a description of the  
27 endovascular intervention task analysis in section 2.1. Section 2.4 describes how the virtual vascular models are  
28 generated. Section 3 presents an evaluation of our IR framework. Finally, discussion and conclusions are presented  
29 in the last section.  
30  
31  
32  
33  
34  
35  
36  
37  
38  
39  
40

## 41 **2. Materials and Methods**

42  
43 The development of ImaGiNE Seldinger was guided and based on the detailed performance of a procedural task  
44 analysis by trained psychologists working with subject matter experts (SMEs). This analysis underpinned the  
45 decision to configure the virtual training environment as two separate workstations, based on a number of factors.  
46  
47 Firstly, the critical importance of the operator's sense of touch to the pulse palpation task required a physical  
48 interface; a mannequin was chosen to represent this. To avoid puncturing and damaging this mannequin at each  
49 training session, a virtual needle was used for actual vessel 'puncture', requiring tracking when manipulated by the  
50 operator during a simulated intervention. The next step required insertion of a real guidewire into the needle hub and,  
51  
52  
53  
54  
55  
56  
57  
58  
59  
60  
61  
62  
63  
64  
65

thence, into the virtual vessel. However, because of the absence of an actual physical needle or puncture / vascular entry site in the mannequin, a second workstation was designed to specifically address guidewire / catheter insertion and navigation.

The first workstation is an immersive environment, using a mannequin in which a simulated pulse is palpated to guide vessel puncture with a needle using an off-the-shelf haptics device (Phantom Omni, Sensable, Woburn, MA). This part of the task terminates when the 'needle' is successfully inserted into the femoral artery, manifested by cueing with a virtual jet of blood issuing from the needle. The second workstation is a virtual simulator that uses two haptics devices to provide a novel interface where a needle can direct a guidewire and catheter within the 'vessel' lumen, guided by touch and virtual fluoroscopy. In this workstation, a novel needle haptics device allows needle orientation by the trainee such that guidewire entry into the virtual vasculature is carried out safely and atraumatically. The trainee then introduces a real guidewire through the needle haptics device into virtual vessels via a proprietary interface device (VSP, Mentice, Gotheberg, Sweden). Completing the training objective finally requires safe passage of the guide wire to the aortic bifurcation.

## **2.1 Task analysis**

The goal of the task analysis was to give a clear description of the core procedural steps of the Seldinger technique and subsequent catheterisation. This description was then used to guide the development of the two workstations to ensure these were fit for purpose in replicating the detailed processes of the intervention and its possible complications. It was also the basis of defining the metrics and the automated assessment tools used in the simulators to evaluate trainee performance. A brief description of the task analysis and metric identification follows. The interested reader can find full details at (Johnson et al., 2011).

To provide the researchers with background information and an understanding of the aims of the procedure, initial discussions were conducted with clinicians, and interventional procedures were observed in situ. Six Interventional procedures using the Seldinger Technique were then filmed using 3 cameras to ensure all aspects of the procedure were captured. One camcorder was fixed on the fluoroscopy screen, a second to acquire an overview of the entire angiographic room, and a third handheld camera to allow constant focus on the clinician's hands. All procedures were performed by SMEs identified as such by the British Society of Interventional Radiology (BSIR) council. Informed consent was gained from all participants and ethical and research governance approval was obtained from

all centres for the completion of this study. Semi-structured interviews were conducted with the clinician following the procedure to develop narration for each part of the procedure filmed. An additional fifteen semi-structured interviews were conducted with other SMEs to provide more detail on the steps and thought processes required during the Seldinger technique. Following the initial interviews, a draft of the task analysis was produced. This was then refined and elaborated on as interviews progressed until a final draft was agreed by both external SMEs and CRaIVE clinical members. The final Seldinger procedure task analysis comprised 81 procedural steps.

The completed task analysis was used to identify critical procedure steps (CPS). These are steps within the procedure, which are critical to its success and are seen to pose a risk to the patient's safety if not completed correctly, making them ideal steps on which to measure performance. A questionnaire was designed using the task analysis asking participants to rate each of the 81 procedural steps in terms of how 'critical' and 'risky' they are. The questionnaire was completed by the SMEs involved in the study, with more participants also recruited to this part of the study at international Interventional Radiology conferences held by industry bodies such as CIRSE (Cardiovascular and Interventional Radiological Society of Europe), SIR (the American Society for Interventional Radiology) and BSIR (British Society of Interventional Radiology). Responses were obtained from 22 experts and the information used to create a list of CPS. The transcripts from the task analysis interviews with SMEs were also reviewed in order to include their views on the most critical parts of the procedure. These CPS were then utilised by the CRaIVE team to develop metrics within the simulator, which could be used to both measure performance on the simulated procedures, and to give detailed performance feedback to participants.

A total of 23 metrics were developed. Important pre-procedural steps (n=6) were included in the simulation through the activation of tick boxes. The remaining 17 were calculated by the simulator during each procedural performance. The following are examples of the metrics used, see (Johnson et al., 2011) for full details:

#### Workstation 1

- Check for Pulse
- How many times did the needle perforate the skin
- Which direction was the needle bevel facing
- Time spent on Workstation 1

## Workstation 2

- Were any calcifications hit in the artery where contrast should have been injected
- How long was fluoroscopy used for
- How much contrast was injected
- Time spent on Workstation 2

### 2.2 Workstation 1: needle puncture

Workstation 1 relates to vascular palpation, local anaesthetic injection and needle puncture. It is developed as an augmented reality environment and composed of a PC workstation, a stereoscopic display frame, a pair of fixed stereo glasses, a mounted PHANTOM Omni and a customized mannequin with an arterial pulse simulator SimPulse-II (Liverpool University, UK) embedded (Fig. 1).

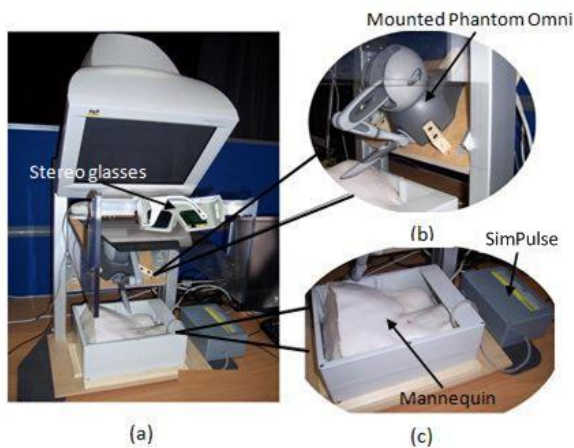


Fig. 1. (a) Configuration of workstation 1. (b) The Phantom Omni haptics device is mounted on the display frame at an angle of 45 degrees from vertical to provide the user with an appropriate range of motion when manipulating the needle. (c) The mannequin and the attached SimPulse provides a tangible interface, the user will be able to feel a programmed pulse. The whole scene is viewed through stereoscopic glasses so that the computer generated imagery (virtual needle, blood flow, etc.) is overlaid onto the scene in 3D.

#### 2.2.1 The mannequin



The mannequin fitted inside a plastic box (300mm long, 230mm wide and 110mm deep) is shaped as the right groin area of the patient. It contains bony structure (e.g. anterior superior iliac spine, the pubic tubercle) made of hard plastic, muscle and fat layer built with flexible expanded foam, skin simulated with silicone gel, and a pulse simulation block connected to a SimPulse-II.

The programmable arterial pulse simulator, SimPulse II, is a hydraulic system used to provide a palpable pulse when locating the common femoral artery. It is able to configure the simulated pulse pressure waveform using adjustable settings, therefore allowing simulating different pulses in terms of frequency and strength.

### **2.2.2 Registration**

Augmented Reality (AR) systems demand accurate registration, since the real world represents a reference frame into which the virtual elements have to be perfectly integrated. Registration errors in AR systems are difficult to adequately control because of the high accuracy requirements and the numerous sources of error. Extending AR system to haptic sense introduces new sources of registration error, which mainly include haptic device workspace distortions and the unknown transformation between the respective coordinate frames. Previous haptic research is concentrated in the areas of tele-manipulation and virtual reality. The work in these areas does not, however, provide insights into the problems of registration with the real scene or interactions between real and virtual objects. The integration of haptic feedback into general AR setups is still fairly new. Early work was conducted by (Grant et al., 1998) and (Ye et al., 2003).

Our work focused on minimizing the overall registration error by reducing geometric distortions in the system. The possible sources of geometric errors for the setup included the individual device workspace distortions and the unknown rigid body transformation between the respective coordinate frames.

To carry out the registration we first adjusted the CRT monitor to limit its geometric distortion and make sure the position and size of the image on the screen is proper; second, the workspace of the haptics device is calibrated by generating a correction grid for the PHANTOM Omni. Third, determining the transformations among different coordinate systems; and, finally, the position of the viewpoint is located. More details of this scheme can be found in [Zhang et al., 2012].

### **2.2.3 Haptics rendering**

The Omni haptics device enables the trainee to feel the resistance of the tissue and the pulse pressure. A virtual needle is overlaid coaxially on the front part of the Omni stylus. When the virtual needle is punctured into the mannequin, force feedback is produced through the Omni.

The force feedback delivered in the AR simulator is an approximation to ~~real procedures~~ measured through a custom-built force sensor, which is detailed in section 2.5. The results of *in vivo* needle puncture force measurements show the force generally increases with the depth of penetration, and local increase and decrease of force appeared as the needle tip punctures through interfaces of different types of tissue, e.g., from air to the skin, from fat layer to blood vessel, etc. Also, when the needle tip is inside the lumen of the blood vessel, the force changes along with the pulse pressure as illustrated in Fig. 2.

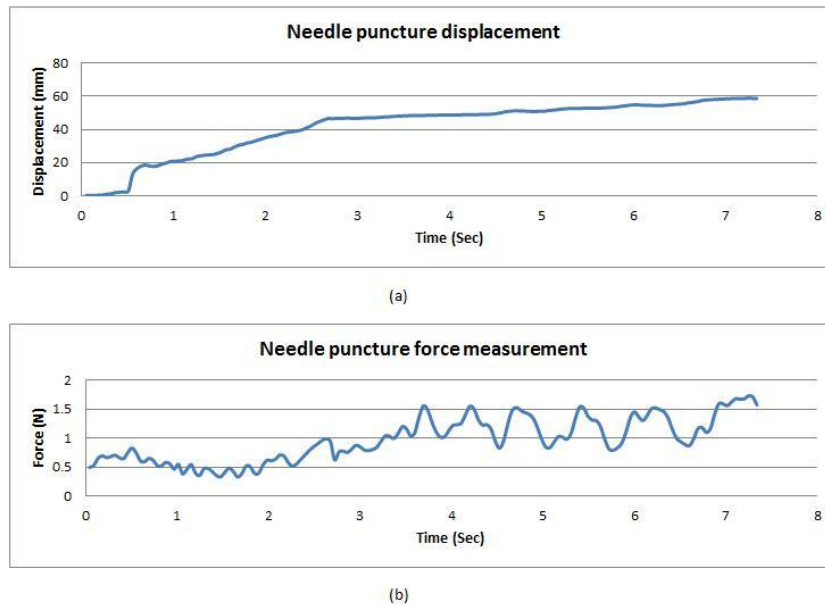


Fig. 2. Needle puncture displacement (a) and force measurement (b)

Needle puncture is an essential component of many clinical procedures. Physically based simulations have been developed for the puncturing of rigid needles [Alterovitz et al., 2003, Vidal et al., 2008] and flexible needles (Chentanez et al., 2009, Peterlik et al., 2011, Goksel et al., 2011, Alterovitz et al., 2005) through several layers of

soft tissue, where needles are simulated as rigid models or 1D discrete flexible models with rigid rods connected by springs, and the use of the Finite Element method (FEM) for tissue deformation has become a de facto standard (Famaey et al., 2008). Most of the simulations consider the force change along with the position and velocity of needle, we know of no prior simulation that handles force changing with time when the needle is still. In our case, when the needle tip is inside the lumen of the blood vessel, even if there is no change in the position, the force felt through the needle can be changed significantly.

To reduce the computation time, the needle is simulated with a rigid model, and the output force of the Omni haptics device is modelled as:

$$F_{needle} = F_{tissue} + F_{interface} + F_{pulse} \quad (1)$$

Where  $F_{tissue}$ ,  $F_{interface}$ , and  $F_{pulse}$  present the reaction force to the tissue resistance as the needle penetrated deeper, the force produced when the needle punctures through interfaces of different types of tissues, and the force caused by the pulse pressure, which varies along time, separately. This haptic rendering model is based on Vidal's 3D rigid needle insertion simulation (Vidal et al., 2008).

The tissue force  $F_{tissue}$  is given by:

$$F_{tissue}(t) = \sum_{i=0}^n k_i (P(t-1) - P(t)) \quad (2)$$

Where  $k_i$  describes a tissue resistance,  $P_t$  is the vector defined by the needle position at time  $t$ .

If the gradient magnitude at the needle tip position in the volume image dataset is higher than a given threshold  $G$ , the needle tip is located at an interface. The interface force  $F_{interface}$  is defined as:

$$F_{interface}(t) = \begin{cases} k_{edge}(P(t-1) - P(t)) & \text{if } g_t > G \\ 0 & \text{if } g_t < G \end{cases} \quad (3)$$

Where  $g_t$  is the gradient magnitude at the needle tip,  $k_{edge}$  describes an interface resistance.

Although there is in general a slight change in pressure waveform amplitudes due to the influence of respiration, etc., cardiac period varies little from beat to beat during a short interval, and can be expressed by the Fourier series written as:

$$P(t) = P + \sum_{n=1}^N P_n \cos(n\omega t - \phi_n) \quad (4)$$

This means a periodic pressure waveform is the summation of a mean pressure component and its sinusoidal or cosinusoidal harmonic components. For an aortic pressure waveform, 10 harmonics are sufficient to accurately reconstruct the waveform (Li, 2004).

In the simulator, the pulse force  $F_{pulse}$  is based on the Fourier expression and given by:

$$F_{pulse}(t) = \begin{cases} \bar{f} + \sum_{n=1}^N f_n \cos(n\omega t - \phi_n) & \text{if } p_t = 1 \\ 0 & \text{if } p_t = 0 \end{cases} \quad (5)$$

Where  $p_t$  represents if the needle tip is inside the lumen,  $\bar{f}$  is a mean force.

## 2.3 Workstation 2: instrument navigation

This virtual simulator is composed of two haptics devices, a display and a PC workstation. Whilst it is mainly aimed at catheterisation training, a key component of the Seldinger technique is incorporated in this workstation and simulated with the first of the two haptics devices: the needle holder and insertion haptics device. This allows positioning of the needle in the correct orientation after vessel puncture in order to facilitate instrument insertion into the vessel. Once a satisfactory angle is reached, the trainee can insert a guidewire, remove the needle and insert a catheter to perform the catheterisation up to the level of the aortic bifurcation. Tracking of these instruments is performed by the second haptics device: the catheterisation haptics device. Both devices are connected to the PC workstation, which uses a mass-spring model to simulate the virtual instruments and their interactions with the virtual vessels. This workstation also receives the motions applied by the user on the instruments and displays them on the screen using a virtual fluoroscopic rendering.

### 2.3.1 Needle holder haptics device

Once the needle has been inserted into the femoral artery in Workstation 1, the trainee must be able to manipulate the needle in terms of orientation, rotation and depth. This step allows modifying the angle and location of the needle tip within the vessel, aligning it with the vessel lumen to facilitate safe entry of the guidewire into and along

the vessel. To this effect, the needle is normally depressed from a position that may be close to perpendicular to the patient, to an angle at or below 45 degrees (being a common approximate angle used for vascular entry), often reducing further to an almost horizontal orientation.

The needle holder haptics device was developed by CRaIVE members at Bangor University (UK Patent Application Number: 1001399.3. European Patent Application Number: PCT/EP2010/066489) to facilitate the above actions

while tracking the motions applied by the trainee to the needle. This interface allows an interventional needle to be inserted and manipulated around a central pivot point using a gimbal design, Fig. 3a. The gimbal consists of two frames, one inside the other and both independently provide a single axis of rotation. Each frame uses an independent precision potentiometer, to locate its position and servo motor to provide force feedback. The complete interface allows for ~~It is composed of two servomotors, each allowing~~ tracking and positioning along the X and Y

axes (Fig. 3b). Because the needle is hollow, the guidewire can be inserted through its centre, but the needle needs to be removed before inserting a catheter, as in the real intervention. Hence, the needle can be inserted or removed from the hub of the servomotors at anytime. A flexible tube directs both the guidewire and catheter from the servos into the catheterisation haptics device. Because the needle haptics device is at a certain distance from the wire/catheter tracking device (Fig. 3c), the needle length is insufficient to engage the tracking device. A tubular conduit is therefore placed at the tip (bevel) of the needle to extend it to allow tracking of the depth and Z rotation of the needle, as well as depth-dependant force feedback, derived from needle force measurements during arterial puncture procedures in patients (see 2.5). This tubular conduit also allows guiding the instruments introduced in the needle towards the VSP to track them during the simulation. Finally, a pressure sensor (hotpot rotary potentiometer model SEN-09074, Sparkfun Electronics) is placed around the servomotors to enable the detection of any operator finger pressure applied close to the needle 'puncture site'. This apparatus is essential to detect if and where the trainee applies pressure on the femoral artery when removing the needle to avoid blood flowing out through the puncture site around the guidewire. This would normally result in a collection of blood (a haematoma) within the tissues. Until a catheter is inserted, the trainee must thus apply pressure above the puncture site.

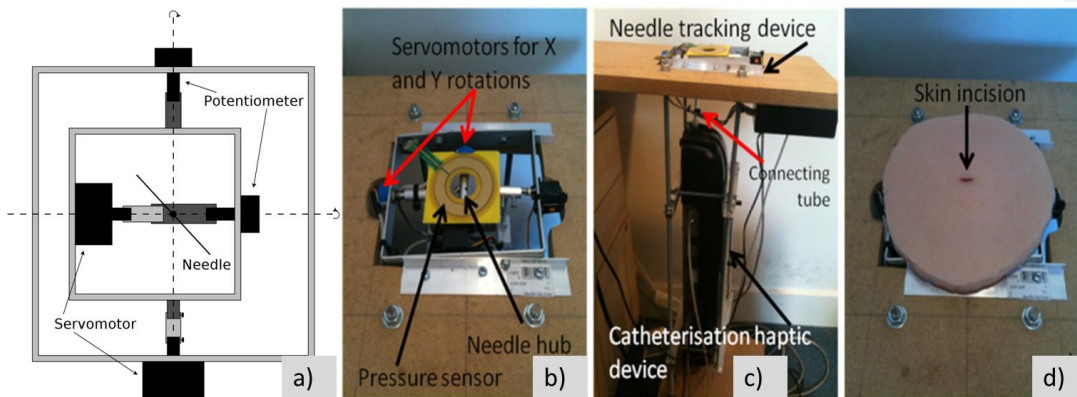


**Fig. 3. a) The needle holder device consists of two frames providing an axis of rotation along their servomotors. b)**

The needle holder haptics device with its servomotor sensors and pressure position sensor. c) Workstation 2 set up with the two haptics devices and the flexible tube channelling the guidewire and catheter inside the catheterisation haptics device. d) Silicon skin with incision to simulate the needle inserted in the artery.

While our first prototype needle haptics device was based on a mouse trackball (Luboz et al., 2009a), our current prototype (Hughes et al., 2011) uses servomotors (Hitech model HS82MG-RC) to accurately position the needle in the same location as that determined from Workstation 1, and precision potentiometers (Vishay model 357-0-0) to get an accurate position of the needle as it is manipulated by the operator. On each axis, the servomotors allow positioning of the needle angle within the range -45 degrees to 45 degrees from the centre point in steps of 1.2 degrees. The potentiometers read the actual position with an accuracy of 0.1 degrees within a tolerance of 3%. The pressure sensor is able to measure the position of the fingers every 0.1 degree ( $\pm 0.02$ ). A calibration phase allows the accuracy to be improved by aligning the components together, resulting in highly accurate rotation axis and pressure position.

To enhance the face validity of the simulator, a layer of silicon with properties (elasticity and colour) similar to the skin has been placed on top of the needle holder haptics device (Fig. 3d). Because the needle puncture has already been made on Workstation 1, the silicon skin presents an incision of 1.2cm that leads to the centre of the servomotors' hub in which the needle is introduced. A ring of silicon on top of the pressure sensor allows better distribution of the finger pressure and, consequently, a better detection of the position of the trainee's finger when

trying to stop the blood spurt while removing the needle. Covering the complete system with a surgical drape further improves the face validity.

### **2.3.2 Catheterisation haptics device**

After the needle angle has been decreased to a satisfactory position, the trainee can start the catheterisation by first inserting a guidewire through the needle. S/he then removes the needle to allow space for the catheter (or an access sheath) to slide over the guidewire, into and within the vessels towards the possible pathology or up to the aortic bifurcation. The catheterisation haptics device is responsible for tracking the guidewire and the catheter during this step. In our framework, we use a commercial device (VSP: Vascular Simulation Platform, Mentice, Gothenberg, Sweden) as shown in Fig. 3c. Real instruments can be inserted into the VSP, enhancing the immersion of the trainee and increasing the realism of the simulation by replicating exactly the sense of touch of a real intervention. The two instruments are simultaneously tracked coaxially during the virtual intervention when the trainee manipulates them with one or both hands, either using dynamic real time virtual fluoroscopic guidance, or an overlaid road map (static, subtracted image). These manipulations consist of translations or rotations that are transferred to the core of the simulator, which then derives the new positions of the virtual instruments within the vasculature in real time. This software has been developed by CRaIVE members at Imperial College London. In addition to computing the position of the instruments, the core of the simulator also computes the forces applied to the instruments in response to collisions with the vessels, and communicates these to the VSP. Forces are then applied as translational frictions to the instruments in order to reproduce the constraints from the vasculature. The amount of friction is proportional to the number of collisions between the instruments and the vessels. This force feedback is also increased or reduced in relation to the total length of the instrument inserted within the vasculature.

### **2.3.3 Catheterisation simulation**

Both haptics devices are connected to the workstation through USB ports. They give the positions of the real instruments, and the simulator displays the motions of the virtual instruments in real time. Physics-based models are used to simulate the behaviour of the instruments. The needle is a rigid object, while catheter and guidewire are represented by mass-spring models as briefly described in the next subsection and in more detail in (Luboz et al., 2009b).

#### *Mass-spring model*

The mass-spring model consists of a set of particles ( $X_0..X_N$ ), of the same mass, connected by stiff springs of equal length ( $\lambda$ ), Fig. 4(a). The first ( $X_0..X_{length}$ ) particles correspond to the instrument's tip, while the subsequent particles ( $X_{length+1}..X_N$ ) represent its body. The tip representation allows modelling the different shapes of the instruments and facilitates the collision response. When an instrument is moved, the motion detected by the VSP is sent to the simulator in the form of translation or rotation.

A translation happens when the instrument is pushed or pulled. To avoid modelling a large number of particles at all times, a mechanism dynamically adds or deletes particles when the instrument is ~~pushed or pulled~~ translated more than the spring length. Real time computation is therefore possible up to a large number of particles. Pulling and pushing are handled differently because of a limitation of the mass-spring model: while pushing the instrument, in some specific collision cases, the instrument tip tended to collapse on itself. To avoid this, an adjustment was introduced to the pushing procedure, helping the tip to be pushed along the axis of its two first particles. On the other hand, when the instrument is pulled, the model behaves intuitively: pulling the proximal particle induces a motion that is iteratively applied to all the other particles of the instrument.

The rotation is handled in an intuitive approach. First, the rotation axis is defined from the last particle of the body to the particle before. Then, the rotation is applied along this axis to all particles. If a collision occurs between a particle and a vessel wall, the collision response (see below) constrains the instrument within the vessel wall and the rotation axis is changed. The new axis is computed between the colliding particle and the next particle. From this particle to the tip, all the particles are rotated along the first axis, then along the new axis. This process is repeated if new collisions happen. The reader is referred to (Luboz et al., 2009b) for further details on the instrument movements.

#### *Collision detection and collision response*

Due to the real time requirement, the collision detection must be computationally efficient and accurate. The vasculature (represented by a triangular surface) is partitioned into an Axis Aligned Bounding Boxes (AABB) tree (created at the beginning of the simulation), while the instrument particles are encapsulated by bounding spheres. When an intersection between a bounding sphere and the tree is detected, the collision detection process determines if there is a collision between the instrument and the vasculature, see (Luboz et al., 2009b) for details on this optimised collision detection algorithm.



Each colliding particle is subject to a collision response ensuring the instrument is maintained within the vessel wall.

Four forces are involved: the external force, spring force, and 2D and 3D bending forces. The external force moves the particle away from the vascular triangles. The spring force ensures that the spring length remains close to its initial length.

The instrument shape is conserved by the 2D bending force, using a bias angle conservation constraint. Only the tip particles have a bias angle in order to shape the different catheters and guidewires. The body particles are initially straight, and therefore have no bias angle. It will consequently contribute to straighten them along all the simulation.

Because in some cases the tip particles might move out of their original plane by the external forces, the 2D bending force is not enough to bring them back to their original position. For this reason, a 3D bending force was added to constrain all the tip particles in the same plane, see (Luboz et al., 2009b) for more details.

#### *Instrument interactions*

During the intervention, the guidewire can move independently, or within the needle or catheter. The catheter can move independently once inserted, or in conjunction with, and over, the guidewire. Finally, the needle moves independently, or with the wire following its insertion into the needle lumen. To model these interactions, different priorities were set on the behaviour of the instruments. The needle's particles override all other instruments to force them to follow the needle rigidly. Outside the needle, the guidewire moves freely. When the needle is removed, the catheter may be inserted and interacts with the guidewire. Since the catheter is over the guidewire, the wire follows its motions. The only exception is when the guidewire has part of its particles outside the catheter. In this case, a motion of the catheter makes the guidewire particles inside the catheter follow it, but the guidewire particles outside the catheter are just updated to satisfy the collision response forces, especially the spring and bending forces. Finally, when the guidewire moves, it influences the catheter's particles depending on the catheter's flexibility. These combinations of interactions lead to the possibility to navigate the instruments inside the vessels and, in particular, to navigate into different arteries to target a pathology. This simple priority approach leads to a fairly accurate behaviour in the main IR cases. Adding complexity in this process, by taking into account different priorities or by adding the flexibilities of the different instruments, could lead to a more accurate simulation but were not integrate in the current simulator as it slowed down the rendering, therefore disturbing the real time interactions.

Different types of instruments are available for IR procedures. They vary widely in length, size, surface coating, material, stiffness, tip shape, etc. Depending on the procedure stage, any range of specific instruments may be chosen. The guidewires can be separated into three groups: access, selection and exchange. Catheters can be either for diagnostic or for therapeutic use. Based on these groups, seven guidewires and three catheters were chosen and modelled in the simulator:

Three access guidewires: Fixed Core Straight (Cook, Bloomington, In, USA), Fixed Core Safe-T-J-Curved (Cook), and Bentson (Boston Scientific, Natick, MA, USA).

Two selection guidewires: Terumo Angled and Terumo Stiff Angled wires (Terumo Europe, Saint Quentin en Yvelines, France).

Two exchange guidewires: Rosen-Curved (Cook, Bloomington, In, USA), Amplatz Super Stiff (Boston Scientific, Natick, MA, USA).

Three diagnostic catheters: 5F Beacon (Cook, Bloomington, In, USA), 4F and 5F Terumo (Terumo Europe, Saint Quentin en Yvelines, France).

## **2.4 Creation of the datasets**

One of the key objectives of computer based simulation is to provide trainees with better access to a wide number of real cases and patient pathologies. To improve the realism of the simulation, it is also desirable to include detailed vascular structures. These targets were achieved by developing a generic application providing fast and precise segmentation of anatomical structures from various patient datasets. Virtual patients can then be generated from the segmentation results.

To date, 28 real virtual data sets have been integrated into our simulator. Following research ethics approvals, 28 patients (mean age 73.21 +/- 10.06, range 52 to 89; 16 males, 12 females) provided consent for use of their medical imaging datasets. These comprised 25 Computer Tomography Angiography (CTA) scans and three Magnetic Resonance Angiography (MRA) scans. The images have an average resolution of  $0.7 \times 0.7 \times 1 \text{ mm}^3$  and typically 600 slices with  $512 \times 512$  pixels.

Fig. 4 shows three examples of virtual patients. For each dataset, the vasculature covers similar vascular anatomical territory: the aorta, renal arteries, iliac and femoral arteries, and inferior elements of cranio-cervical vessels. One of

the datasets is non pathological, while the others offer a wide range of pathologies, including aortic aneurysm, aortic dissection and femoral and iliac arterial stenosis. This large variety of virtual patients gives the trainee the opportunity to try different approaches and different instruments in the virtual world, and to acquire the necessary experience to improve his/her skills before moving to real interventions.

Manual and interactive segmentation methods are not well suited to tasks where a huge number of slices and amount of detail need to be processed. Many automatic or semi-automatic vascular segmentation techniques have been proposed and implemented in recent years. However, texture-based approaches which are mainly based on local intensity or intensity gradient features are not sufficient to cope with this study, since our datasets are from different sources using protocols that vary in quality and resolution. Although many well-known model-driven, knowledge based image analysis approaches, like (Gao et al., 1998), incorporate prior knowledge about mean shape of anatomies from which to capture natural variations, this study focuses on patient datasets presenting typical pathologies. It therefore needs to handle abnormalities, even some extreme shape deformations which would not be captured by a standard shape model. Sethian (1999) proposed a level set method to model arbitrarily complex shapes without priori assumptions about the topology of an object. It can therefore capture the range of shape variations and anomalies required by our application.

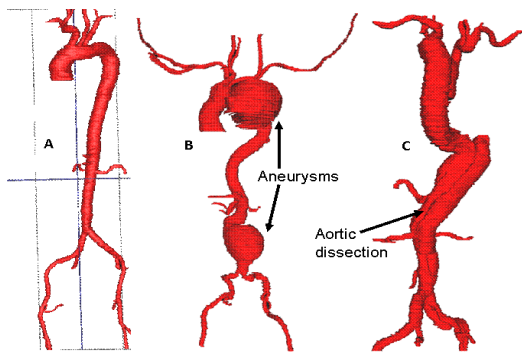


**Fig. 4.** Three different anatomies of the studied vasculature from femoral arteries (inferiorly) to aorta (in the middle) to neck vessels (superiorly): A. non pathological aorta, B. two aortic aneurysms, and C. aortic dissection

A large body of work has explored the level set method and its applications to medical image segmentation (Droske et al., 2001, Watanabe et al., 2002). Most approaches require complicated parameter tuning and the need to place relatively large amounts of seed points at appropriate positions. Thus requiring users to have sufficient mathematical

and anatomical knowledge. Consequently, the segmentation result is also sensitive to parameters setting, seed positions and seed numbers. Furthermore, while improving the ability to model complex shapes, the problem of introducing “leaking” at the boundaries of objects of interest becomes unavoidable.

To overcome the shortcomings of the traditional level set approaches, we propose a novel approach (Song et al., 2008) replacing seed placement by a region model, which is a close approximation to the actual desired structure. With the region model, our level set implementation can increase the chances of segmenting a complex object without missing details; and can significantly reduce the time of convergence, thus reducing “leaking” during the level set evolution process. Another advantage of our region model based level set method (RMLS) is a lack of sensitivity to parameter settings. Default parameters are applied without the need to tune for each case.

Our method generates the region model by applying morphological erosion on an edge enhanced image followed by a region growing algorithm. Fig. 5 illustrates our edge enhancement algorithm. The gradient magnitude of image  $I_1$  (Fig. 5a) at each pixel is computed (Fig. 5b) and a lower hysteresis threshold  $T$  is applied to the result to suppress spurious edges (Fig. 5c).  $T$  is estimated using the histogram of the gradient image. The remaining edges are enhanced to the maximum intensity value  $C$  of image  $I_1$ , (Eq. 6).

$$I_1'(x) = \begin{cases} C & \text{if } \nabla I_1(x) > T \\ 0 & \text{else} \end{cases} \quad (6)$$

Mathematical morphology operations are then applied on the enhanced image  $I_2 = I_1 - I_1'$  (Fig. 5d) and capture the major object structures to form the region model which is then embedded into the level set function  $\Psi(x, t=0)$  (Eq. 7) for further refinement.

$$\frac{d}{dt} \Psi + \alpha P |\nabla \Psi| - \beta K |\nabla \Psi| = 0 \quad (7)$$

The propagation term  $P$  from Eq. 7 is an image based force defined from the feature image  $g(I)$  (Fig. 5e), which is computed by using a region competition method (Zhu and Yuille, 1996). A study of the performance of our method is presented in (Song et al., 2011).

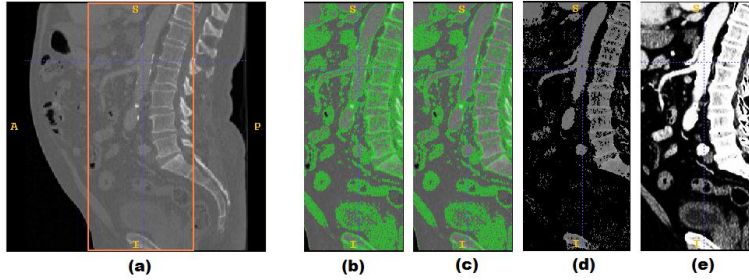


**Fig. 5.** Edge enhancement. (a) Original slice in sagittal view (image  $I_1$ ). The area inside the rectangular box indicates the location of the abdominal aorta. (b) The gradient magnitude of image  $I_1$  (only partial image  $I_1$ , i.e. the area inside the rectangular box of (a) is displayed). (c) Spurious edge suppression. (d) Image  $I_2$  after subtracting the enhanced edge from image  $I_1$  (e) Feature map of image  $I_0$ .

## 2.5 Needle puncture force and instrument flexibility measurements

The needle puncture force was measured through a custom-built force sensor (Fig. 6). Its sensing principle relies on a cantilever beam mounted with four semiconductor strain gauges (Micron Instruments, Simi Valley, California, USA). The beam is with an integral frame machined from one piece of aluminium and has a circular hole of diameter 5mm in the middle. An aluminium tube that fits into this hole is securely bonded onto the beam. A male Luer connector is fixed to the bottom cover. The bottom section of this connector mates with the hub of a vascular access needle and the top section passes through the beam and the hollow tube, but without making direct contact with either. The top cover has a clearance hole for the central tube, which protrudes through the cover by 5mm. A needle hub (the 'holder') is carefully removed from a vascular access needle and secured within the central tube. The strain gauges and the wiring inside the sensor are covered with thin layers of water-resistant compounds (Gagekote #5 and Gagekote #8, Vishay Measurements Group UK Ltd, Basingstoke, UK) to protect them from blood contamination during *in vivo* use and from cleaning after the measurement.

During operation, a vascular access needle is firstly connected to the Luer connector of the sensor. The operator holds the sensor casing or the needle hub 'holder' and moves the needle towards the skin above the femoral artery of the patient. Forces are constantly recorded during the insertion of the needle, until a gush of blood jets through the end of the holder hub, indicating a successful arterial puncture.

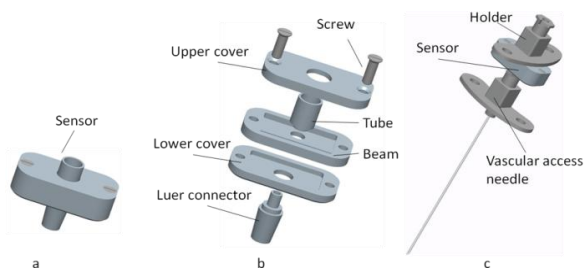


**Fig. 6.** Needle puncture force sensor. (a) Assembled force sensor. (b) Sensor exploded view with the cantilever beam, lower and upper covers. (c) Sensor and top hub holder connected with a vascular access needle.

The validation of the force sensor was carried out using a tensile tester (Nene Instruments Ltd., Wellingborough, UK) fitted with a 5N load cell during needle puncture of porcine liver, kidney and subscapularis muscle. The load cell was connected to the holder of the force sensor whilst an 18G 2-parts Kimbal needle was inserted in the Luer connector of the sensor. Downward movement of the crosshead of the tensile tester caused the needle to penetrate through the tissues at a constant speed whilst the load signals from the load cell and the needle sensor were recorded continuously. These results from the two different methods were analysed using Bland-Altman plot. The correlation coefficients for all tissues are higher than 0.996, which indicate high degree of agreement.

The instrument flexibility was determined by measuring the flexural modulus of seven commonly used guidewires (See the quantitative evaluation in section 3.2), along the wire's length. A three-point bending test was used for the main body, while a two-point test was used for the floppy tip of the wires. In the three-point test, the wire to be investigated was placed on a jig comprising two supports 4cm apart; a probe was used to apply force to the centre of the wire. The wire was depressed 5mm by the probe at a speed of 25mm/min and the force exerted on the probe was recorded. A two-point bending test was used for the floppy tip section of the wires. During the test, the wire was clamped at one point and the probe applied 1cm away from the clamp, to deform the wire with a maximum deflection of 2mm while recording forces generated.

Seven guidewires of each type were tested using these two methods. The recorded force data were used to calculate the flexural modulus of the wires at each point. Results show that the flexural modulus of the tested wires ranges from 55MPa at the floppy ends, to 66GPa at the main body.

### 3. Results

The combination of the two workstations provides the first virtual training environment for the Seldinger technique and navigation of instruments inside the vasculature through the needle puncture site. Its evaluation has been separated into three steps: an evaluation of the performance of each workstation and a validation study of the whole environment.

### 3.1 Workstation 1: needle puncture

The mannequin enables the trainee to palpate the bony landmarks and locate a rough position of the femoral artery. The simulated pulse then gives a more accurate indication of the position of the blood vessel. The silicon skin, foam fat and muscle layer, and the plastic bones in the mannequin provide a realistic feeling. Because of the tissue layers, the default pulse setting produced by the SimPulse was considered to be too weak when it was palpated from the skin of the mannequin. In the evaluation, the frequency and strength of the pulse was adjusted to simulate the situation of the selected patient.

The virtual needle is calibrated to align with the centre line of the Omni stylus, and the centre point of the needle wings is registered to the tip of the Omni stylus. With this configuration, the virtual needle can be fully inserted into the mannequin without interaction between the Omni stylus and the mannequin. Using the method mentioned in section 2.2, we achieved 0.5 degree accuracy on the angle alignment between the virtual needle and the centre line of the Omni stylus and 3mm accuracy on the translate calibration.

In Workstation 1, the stereoscopic glasses are fixed to the stereoscopic display frame, which limited the users' viewpoint. However, viewpoint positions of different users can still change significantly even though they observe the augmented virtual environment through the fixed glasses. To achieve a precise registration for an AR environment, it is important to estimate the viewpoint offset accurately. Instead of measuring the offset in each procedure, a view-based approach is used to guide the user to the preset viewpoint position in the evaluation.

Parameters in the needle puncture force model have been adjusted to match the trend of the *in vivo* force measurement data. *In vivo* forces are measured for five patients, with depths of blood vessel below skin range from 70mm to 150mm. For each patient, two punctures are repeated; parameters in  $F_{\text{tissue}}$  and  $F_{\text{interface}}$  are estimated using a non-linear least-squares algorithm; and parameters in  $F_{\text{pulse}}$  are estimated using Fourier Transform. In the final force model, average values over patients of the parameters in  $F_{\text{tissue}}$  and  $F_{\text{interface}}$  are adopted, and those parameters in  $F_{\text{pulse}}$  are correlated to the settings in the SimPulse. The accuracy of the needle puncture force simulation is demonstrated

evaluated by comparing against *in vivo* force measurement data acquired during those punctures on actual patients.

One of the results is illustrated in figure 7 and shows good correlation. The different  $k_t$  describing the tissue resistances, were determined to fit this 5 patient force measurement data.

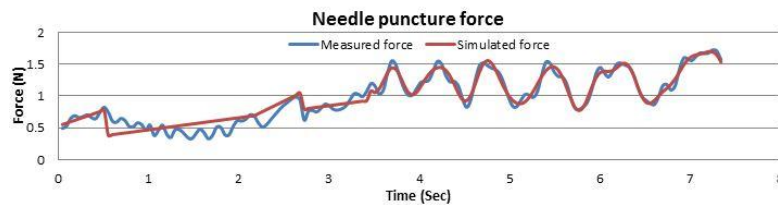


**Fig 7.** Comparison of the simulated needle force measured and the needle force measured during a puncture on a patient and simulated needle force

The force model also simulates higher forces when the needle is puncturing a bone or when fully inserted.

When the tip of the virtual needle is inside a blood vessel, a virtual blood jet is simulated using particles. There are four types of blood jet which represent four needle positions: needle bevel partly inside an artery lumen; needle bevel fully inside an artery lumen; needle bevel partly inside a venous lumen; needle bevel fully inside a venous lumen. When the blood jet representing the needle bevel fully inside an artery lumen is displayed, the task for Workstation 1 is successfully finished. The metrics for Workstation 1 are computed and transferred to Workstation 2.

### 3.2 Workstation two: instrument navigation

Positioning the needle haptics device in front of the VSP enhances instrument navigation by the addition of needle interaction with instruments, and therefore more realistic training of the basic skills. This prototype is the first environment to allow such training. More details are given in (Hughes et al., 2011). It permits exploring and practicing various strategies of needle access into blood vessels, the influence of needle angle on guidewire insertion, and the process of needle / catheter exchange. Thanks to a precise set up, both haptics devices lead to an accurate tracking of the actions and motions by the trainee.

The needle holder haptics device tracks needle rotation on the X and Y axes. The rotation on the Z axis and the depth are tracked by the VSP. The servomotors/potentiometers allow the needle to be rotated  $\pm 45$  degrees from the centre point on both X and Y axes. The servomotors position the needle within 1.2 degree steps and the potentiometers read the actual position with an accuracy of 0.1 degree within a tolerance of 3%, which is sufficient

Formatted: Subscript



for all needle puncture simulations. It allows accuracy in: (1) determining completeness of needle insertion into the vessel and error in missing it (either too deep or too shallow), (2) the angles of insertion, (3) the needle position before inserting the next instrument, and (4) automatic positioning of the needle according to the coordinates recorded in Workstation 1. A further advantage is the activation of the servomotors in a periodic motion to simulate a pulse transmitted to the needle, increasing realism. Hence, this unique haptics device provides a new interface to simulate and assess the way the trainee accesses the vessel during the Seldinger technique. Experts considered this a very useful device for the training of novices in the Seldinger technique.

During the simulated procedure, bleeding is recreated through a set of flashing red lights. A linear array of 8 tri-Coloured Light Emitting Diodes (LED) has been added next to the needle tracking device. Once the needle is in a satisfactory position, the trainee's insertion of the guidewire into the needle prevents bleeding through the needle lumen. Once the VSP is able to track the instruments, they can be displayed in the simulator and the trainee can navigate in the virtual vasculature.

The task analysis has determined that the guidewire must be inserted at least 5 cm before the needle is removed from the puncture site, to avoid the guidewire being removed from the vessels by accident. A simulation loop controls this metric and triggers bleeding (i.e. the flashing red LED) again when the needle is removed (real world bleeding occurs through the space around the wire). To prevent this bleeding, the trainee must press on the top of the puncture site: this action is tracked by the pressure sensor around the needle tracker. This sensor identifies the location of the applied pressure in 0.1 degree ( $\pm 0.02$ ) steps, and therefore allows a very precise localization of the pressure applied by the trainee. A metric checks whether the trainee pressed effectively, i.e. over the puncture site which represents the correct location. Bleeding is therefore 'stopped' if the pressure is correctly applied directly over the needle puncture hole in the vessel wall.

After the needle is removed, the catheter can be inserted. The selected guidewire and catheter are recorded to compare the trainee's choices with the ideal procedure. During the virtual intervention, the metrics described in section 2.1 are computed. They are displayed at the end of the procedure to give feedback to the trainee.

A quantitative evaluation was performed in two separate studies. In (Luboz et al., 2011a), the integration of real guidewire flexural modulus measurements into our simulation framework was presented. The 2D bending parameter,  $k_b$ , of the mass-spring model described previously is used to simulate the flexural modulus of the wires for the tip and the body. In the above study,  $k_b$  was adjusted for each guidewire to match the virtual instrument to their real

counterpart while navigating in a silicon rubber vascular phantom filled with a soapy solution to reduce the friction of the silicone close to the one of blood vessels. Furthermore, this solution allows modelling the change in flexibility due to the hydrophily of the instruments. The three other coefficients, related to the external force, the spring force and the 3D bending force, are constant for all instruments ( $k_e = 1$  for the body particles and 0.9 for the tip particles,  $k_s = 1$  for every particle, and  $k_{b3D} = 1$  for the tip and 0 for the body) and therefore have only a minor influence on their flexibility. To show the similarity of the real and virtual guidewires, the Dice Similarity Coefficient (DSC) (Zijdenbos, 1994) was determined at several insertion lengths in 2D snapshots of the vascular phantom. On average, at the maximum insertion, the real and virtual guidewires are 42% similar. For example, the real and virtual Cook Straight guidewires are 47% similar at their maximum insertion. Accuracy is indicated by the maximum distance measurement between each real and virtual wire, which shows a maximum separation of 2mm. Recently, we also determined the catheters' flexural moduli experimentally and improved our parameterization of the guidewires in (Luboz et al., 2011b). The same silicone rubber vascular phantom was used to compare the instruments while being inserted inside a CT scanner to allow a three-dimensional evaluation. Results showed good correlation with an average distance of 2.27mm between the real and virtual instruments, with a standard deviation of 1.54mm. As shown in Fig. 8, some errors still appear, especially at the tip of the instrument. Nevertheless, for most of the instrument particles there is at least an intermediate agreement (less than 2mm distance between real and virtual instrument for 62% of the particles).



**Fig. 8.** Comparison of the real (black) and virtual (different colours) Terumo angled guidewires in the silicon rubber phantom. The insertion point is on the left and the tips are on the right. The virtual wire particles are blue when there is very good agreement (< 0.5mm), green for good agreement (> 0.5mm, < 1mm), yellow for an intermediate agreement (< 1mm, > 2mm), orange for a poor agreement (> 2mm, < 3mm) and red for a very poor agreement (> 3mm).

No quantitative evaluation of the interactions between instruments was done as it proved to be difficult to differentiate a catheter and a guidewire on a CT image. Nevertheless, several instruments were tested by experienced interventional radiologists in the simulator and they agree that the instruments interact realistically in the first arteries of the virtual vascular models available in workstation 2. The needle indeed overrides any instruments within its tube, while the catheters and guidewires allow guiding the tip of the foremost instrument inside the vessels.

In terms of computational efficiency, the collision detection algorithm implemented, facilitates the running in real time of our virtual catheterisation framework. Two instruments can be simulated with a frame rate over 30FPS using up to 700 particles each, while interacting with a highly detailed vascular model of 80,000 polygons, on a laptop equipped with a Pentium M 1.8GHz and 2GB main memory. With a spring length of 2mm, it corresponds to an instrument of 1400mm, which is a common overall length of guidewires and some catheters.

In terms of forces, the force sensor presented in 2.5 was used to give a first estimate of the force used to push and pull an instrument inside the simulator and inside a real patient. In this first estimation, the force sensor was attached to a guidewire and it was followed while performing real and virtual procedures. During a real intervention, on average, a force of -2 N is monitored when pulling the guidewire away from the patient, while a force around 2.5 N is recorded when pushing the instrument inside the patient. To control the force applied to the instrument in the virtual intervention, it is possible to set a friction coefficient on the instrument using the VSP. We therefore set forces to match those recorded with the force sensors. We reached level similar to the ones presented above within 0.5 N. These virtual forces can be changed by adapting the friction coefficients for each of the different guidewires and catheters to simulate real instruments' forces.

### **3.3 Validation**

A first evaluation of the simulator was carried out during a UK meeting of expert vascular interventional radiologists. Several experts (n=10) tried our simulator using some of the 28 available datasets and provided an initial evaluation before the full validation study. For workstation one, they reported that the variation of simulated forces corresponding to the needle puncturing through skin and blood vessel, and the force changes along the pulse pressure are realistic. As for workstation 2, the behaviour of the instruments was considered close to the real

procedure in terms of translation, rotation and force feedback. Furthermore, the needle haptics device was thought to be a useful approximation for the Seldinger technique. The complete set up was qualified as realistic and accurate.

The simulator has been evaluated in a validation study conducted across six UK hospitals in order to determine the relevance of the metrics, incorporated in the simulator, in terms of acceptability (face validity), performance assessment (construct validity) and the effectiveness of the simulator as a training tool (predictive validity). Face validity results were based on responses from fifty-two participants who completed at least two trials of the simulated Seldinger procedure. Participants were asked to rate the simulator on forty-five items using a seven-point response format ranging from 'strongly disagree' to 'strongly agree'.

Twenty-nine of the items assessed participants perceived in terms of realness of the individual simulator features and fifteen items assessed participants' perceptions about the utility of the simulator as a training tool. Overall, in the case of thirty-three items out of the forty-four, more participants agreed than disagreed indicating acceptance in terms of realness and utility of the simulator.

Participants rated the items listed below as most realistic with more than 69% of participants agreeing with the item:

- The use of the Fluoroscopy pedal (98%)
- The location of the bony landmarks in the mannequin (78%)
- The pulse location in the mannequin (71%)
- The response of the manipulation of the wire on screen (70%)

The acceptability of the simulator as a training tool is indicated from the responses below:

- The simulator would be effective for learning basic skills of the procedure (78%)
- It would be useful in learning how to use equipment (86%)
- The simulator offers a user-friendly environment (75%)
- The simulator was fun to use (84%)

The construct validation process involves comparing the performance as measured by the metrics, across different levels of experience in Interventional Radiology. Data was collected from Radiology Registrars, experienced Interventionalists as well as Vascular Surgeons to ensure the full spectrum of expertise was represented within the sample (N=64). It was expected that experienced participants would outperform less experienced participants on the individual metrics. The outcome of this construct validation determines whether the incorporated metrics function as

an objective assessment tool. For the purposes of the present analysis, metrics which were represented through tick boxes were not included in the analysis. Two further metrics ('Which direction was the needle bevel facing' and 'Was pressure applied to the skin nick to stem bleeding when the needle was removed') were excluded as they did not operate correctly within the simulator. Thus analysis was based on the remaining fifteen metrics.

In order to compare group performance across years of experience in Interventional radiology the participants were split into two groups, group 1 consisted of participants with 0 to 4 years experience ( $n=41$ ) and group 2 consisted of participants with 5 or more years of experience in Interventional Radiology ( $n=23$ ). The results from the analysis of the continuous metrics are displayed in table 1. Results showed a significant group difference for the performance metric of 'How many needle passes were made through the artery',  $t(59) = 2.59, p = 0.013$  and 'Time taken on Workstation 1',  $t(59) = 2.46, p = 0.017$  with the more experienced group on average making less needle passes through the artery than the less experienced group and needing less time to complete the procedure. Although not significant, a trend in the expected direction emerged for five further metrics: 'Needle passes through the skin', 'Number of no go areas hit', 'Number of times the catheter went over the tip of the wire', 'How long fluoroscopy was used for' and 'Time taken on WS2'. It should be highlighted that on the catheter metric none of the participants from the more experienced group went beyond the wire tip with their catheter while the less experience group on average went 2.24 times beyond the wire tip with the catheter. A significant group difference in the unexpected direction was found for the metric of 'percentage of bleeding evident',  $t(58) = -2.62, p = 0.011$  with the less experienced group performing better (lower percentage of bleeding evident) than the more experienced group.

The frequency values for the metrics measured in a dichotomous format were analysed using Chi Square Analysis (see tables 2 and 3). As displayed in table 2, there was a significant relationship between years of experience and the position of the needle tip in the femoral artery,  $\chi^2(1, N = 61) = 10.51, p = 0.01$ . It can be seen from the output below that 82.6% of the more experienced participants punctured within the CFA compared to 76.3% of the less experienced group. However a larger percentage of the less experienced group (47.4%) punctured in the perfect position of the mid 3<sup>rd</sup> compared to only 13% of the more experienced operators.

There was a significant relationship between years of experience and the handling of the catheter,  $\chi^2(1, N = 60) = 4.28, p = 0.05$  (table 6). None of the experienced group advanced the catheter tip over the tip of the wire compared with 19.5% of the less experienced group.

Preliminary results from twenty-six radiology registrars who completed four trials on the simulator, showed that, on average, participants' performance improved over the four trials on all metrics, apart from 'Distance between the anaesthetic and the puncture site'. Significant performance improvement was found for 'Needle passes through the skin', 'Time taken on Workstation 1', 'Were any calcifications hit in the artery where contrast should have been injected' and 'How long was fluoroscopy used for' (see Table 4). However, it cannot be assumed that skills acquired on a simulator automatically extend to real life. Thus, predictive validity was investigated through assessment of skill transfer to procedures undertaken in patients using a randomised control trial study design.

Table 1. Comparison of continuous metrics by years of experience in IR (\* Significant at 0.05 level)

Performance metric	Mean (sd)		T	p
	Group 1	Group 2		
Needle passes through skin (count)	11.48 (9.08)	9.39 (6.61)	0.958	0.342
Needle passes through artery (count)	48.76 (64.60)	20.26 (15.81)	2.594	0.013*
Distance between anaesthetic and puncture (mm)	11.82 (10.61)	15.39 (14.77)	-1.097	0.277
Number of no go areas hit (count)	1.66 (1.05)	1.57 (1.04)	0.336	0.738
Time taken on WS1 (s)	7.28 (4.40)	4.76 (2.78)	2.458	0.017*
How many times did catheter tip go over wire tip (count)	2.24 (8.91)	0.00 (0.00)	1.612	0.115
How long was fluoroscopy used for (s)	66.34 (38.79)	55.35 (29.44)	1.211	0.232
How much contrast was injected (ml)	1.00 (0.71)	1.16 (0.50)	-0.875	0.385
Time taken on WS2 (s)	5.22 (1.64)	4.84 (0.94)	0.944	0.349
How long was bleeding evident (s)	23.59 (18.93)	29.64 (20.04)	-1.131	0.263
Percentage of the time bleeding was evident (%)	38.04 (28.51)	58.41 (26.95)	-2.619	0.011*

Table 2. Performance comparison for 'Where in the femoral artery was the needle puncture site' by years of experience in IR. Chi Squared=10.510, df =2,  $p < 0.05$

Years of Experience	Position of needle tip		
	CFA Mid 3 <sup>rd</sup>	CFA (not mid 3rd)	Not in CFA
	Count (%)	Count (%)	Count (%)
0-4 Years	18 (47.4)	11 (28.9)	9 (23.7)
5+ Years	3 (13.0)	16 (69.6)	4 (17.4)

Table 3. Performance comparison for ‘Did the catheter tip ever go over the guide wire tip’ by years of experience in IR

Years of Experience	Did the catheter go over the wire tip	
	No	Yes
	Count (%)	Count (%)
0-4 Years	33 (80.5)	8 (19.5)
5+ Years	19 (100.0)	0 (0.0)

Chi Squared=4.278, df =1, p<0.05

Results from the complete study, encompassing face, construct and predictive validity, will be published once the validation study is complete and sufficient data has been collected to produce robust results. If successful, this will form a strong evidential base for the simulator to be incorporated into the training curriculum of IR.

Table 4. Mean values for metrics with significant performance improvement († Values from trial two and trial four were compared for these metrics to avoid bias, as no calcifications can be hit in the patient data from trial one, \*\* p < .01, \* p < .05)

Metric	Mean Trial 1	Mean Trial 4
How many times did the needle perforate the skin	11.5**	4.1**
Time spent on Workstation 1	7.7**	2.4**
Were any calcifications hit in the artery where contrast should have been injected †	19.7*	6.7*

How long was fluoroscopy used for †	107.7*	77.0*
-------------------------------------	--------	-------

Overall, non-significant group differences were prevalent, albeit in the expected direction for seven of the metrics ('Needle passes through the skin', 'Number of no go areas hit', 'Number of times the catheter went over the tip of the wire', 'How long fluoroscopy was used for', 'Time taken on WS2', 'Distance of local anaesthetic from the puncture site' and 'Position of needle tip'). However significant group differences with experienced participants performing better than less experienced ones were found for two of the performance metrics ('Needle passes through the artery' and 'Did the tip of the catheter go over the wire tip'). Whilst the two significant results in the expected direction do lend support to the validity of these metrics the analysis for the remaining seven measures is less clear suggesting further research is required, the results of the predictive validity study may also offer further evidence as to the utility of these metrics as training tools.

#### 4. Conclusion and discussion

This paper has presented ImaGiNe Seldinger, a novel virtual environment for teaching the core skills of vascular interventional radiology: from gaining access into a vascular structure by a needle (Workstation 1), through which a guidewire is inserted, thereby allowing introduction and navigation of guidewires and catheters within the vascular tree (Workstation 2). This environment allows training of future clinicians before they attempt this task in patients within the traditional apprenticeship, potentially reducing risk to patients and training cost. A task analysis of the procedure guided the development of the two workstations in terms of key interventional steps and evaluation metrics. Workstation 1 uses an immersive environment, composed of a mannequin in which a simulated pulse is palpated to guide vessel puncture with a needle using a haptics device. It leads to the insertion of the virtual needle into the femoral artery. Workstation 2 uses two haptics devices to navigate needle, catheter and guidewire within the vessels, guided by virtual fluoroscopy. The first haptics device is a novel device tracking the needle orientation. The second haptics device is a commercial device. The complete environment provides different training experiences in terms of anatomy and complexity through 28 real patient datasets. Fidelity of the simulation is enhanced by the integration of real instrument properties and tissue measurements.

Initial evaluation of the complete environment was carried out by interventional radiologists. They found that the set up was realistic and reasonably accurate. Moreover, a quantitative evaluation of the instrument behaviour showed



that, on average, the real and virtual guidewires have a DSC of 42%. Although this value does not indicate an excellent match (above 70% has been cited as excellent (Zijdenbos et al., 1994)), our measurement can be regarded as a satisfactory match, given the difficulty of matching wires of small diameter. This is proven by the average distance of 2.27mm between the real and virtual instruments with a standard deviation of 1.54mm (Luboz et al., 2011b). This value could be reduced even further if the tip is modelled more accurately, possibly by using a variable 2D bending coefficient for the tip particles. Nevertheless, these figures highlight the accuracy and realism of our virtual instruments.

Further evaluation is in progress through the validation of ImaGiNe Seldinger, which aims at determining its construct validity and its predictive validity. Preliminary validation results suggest that our simulator is a valid training environment. It is acceptable as a training tool: with 82% agreeing that the simulator would be effective for learning basic skills of the procedure, 86% believing it would be useful in learning how to use equipment, and 75% agreeing that the simulator offers a user-friendly environment. Moreover, users' performance improved over the four trials on all metrics during our tests. Even though these preliminary results are extremely encouraging, they do not mean that skills acquired on our simulator will automatically extend to real life procedures. The validation process will therefore continue to investigate the transferability to real procedures.

Future works will aim at improving the navigation suite, in terms of catheter and guidewire models, using Cosserat rods which would lead to a more realistic simulation. Trying to couple the two workstations will also be a major challenge which yet needs to be overcome.

## Acknowledgments

This work was partially funded by the Engineering and Physical Sciences Research Council (EPSRC) in the United Kingdom.

## References

1. SELDINGER S.I., 1953. "Catheter replacement of the needle in percutaneous arteriography; a new technique". Acta radiol. 39(5):368-76.
2. Seymour N.E., Gallagher A.G., et al, 2002. "Virtual reality training improves operating room performance: results of a randomized, double-blinded study". Ann. of Surgery, 236: 458-463.

3. Rowe R., Cohen R., 2002. "An evaluation of a virtual reality airway simulator". *Anesthesia & Analgesia*, 95:62–66.
4. Chaer R.A., DeRubertis B.G., et al , 2006. "Simulation improves resident performance in catheter based intervention". *Ann. Surgery*. 244 (3)343-349.
5. Coles T. R., Meglan D., John N. W., 2011. "The Role of Haptics in Medical Training Simulators: A Survey of the State of the Art". *IEEE Transactions on Haptics*, vol. 4, no. 1, pp. 51-66.
6. Mayooran Z., Watterson L., et al., 2006, "Mediseus Epidural: Full-Procedure Training Simulator for Epidural Analgesia in Labour," *SimTecT Healthcare Simulation Conference*.
7. Dang T., Annaswamy T.M., et al., 2001, "Development and Evaluation of an Epidural Injection Simulator with Force Feedback for Medical Training," *Stud Health Technol Inform*, 81, pp. 97-102.
8. Vidal F.P., John N.W., et al., 2008, "Simulation of Ultrasound Guided Needle Puncture Using Patient Specific Data with Textures and Volume Haptics," *Comp. Anim. Virt. Worlds*, 19 (2), 111-127.
9. Chui C.K., Li Z., et al., 2002. "Training and pretreatment planning interventional neuroradiology procedures – validation". *MMVR*, 85, 96–102.
10. Cotin S., Duriez C., et al., 2005. "New approaches to catheter navigation for interventional radiology simulation". *MICCAI*, 8, 534-542.
11. Alderliesten T., Konings M., et al., 2007, "Modeling Friction, Intrinsic of Curvature, and Rotation Guide Wires for Simulation of Minimally Invasive Vascular Interventions". *Trans. Biomed. Eng.*, 54 (1).
12. Johnson, S. J., Guediri, S., Kilkenny, C., Clough, P., 2011. Development and Validation of a Virtual Reality Simulator: Human Factors Input to Interventional Radiology Training. *Human Factors*, 53 (6), 612-625, DOI 10.1177/0018720811425042
13. Grant, B., A. Helser, et al. (1998). Adding Force Display to a Stereoscopic Head-Tracker Projection Display. *Proc. IEEE Virtual Reality Ann. Int'l Symp. (VRAIS '98)*: 81-88.
14. Ye, G., J. J. Corso, et al. (2003). Vishap: Augmented reality combining haptics and vision. *IEEE Intl. Conference on Systems, Man and Cybernetics*: 3425--3431.
15. Zhang Y., Ward J., 2012. An efficient calibration and registration scheme for haptic augmented reality based medical training system, submitted to *Computer Methods in Biomechanics and Biomedical Engineering*.

16. Alterovitz, R., Pouliot, J., Taschereau, R., Hsu, I.-C., and Goldberg, K. 2003. Simulating needle insertion and radioactive seed implantation for prostate brachytherapy. In *Medicine Meets Virtual Reality 11*, IOS Press, 19–25.
17. Chentanez N., Alterovitz R., Ritchie D., et al., 2009. "Interactive Simulation of Surgical Needle Insertion and Steering". In *Proceedings of ACM SIGGRAPH 2009*, pages 88:1-10.
18. Peterlik I., Nouicer M., Duriez C., Cotin S., et al., 2011. Constraint- based haptic rendering of multirate compliant mechanisms. *IEEE Trans. Haptics*, Special Issue on Haptics in Medicine and Clinical Skill Acquisition, vol. 4, pp. 175-187.
19. Goksel, O.; Sapchuk, K.; Salcudean, S.E., 2011. "Haptic Simulator for Prostate Brachytherapy with Simulated Needle and Probe Interaction," *Haptics*, *IEEE Transactions on* , vol.4, no.3, pp.188-198.
20. Alterovitz, R., Goldberg, K., and Okamura, A. M. 2005. Planning for steerable bevel-tip needle insertion through 2D soft tissue with obstacles. In *IEEE International Conference on Robotics and Automation*, 1652–1657.
21. Famaey N. and Sloten J.V., 2008, "Soft Tissue Modelling for Applications in Virtual Surgery and Surgical Robotics," *Computer Methods in Biomechanics and Biomedical Eng.*, vol. 11, no. 4, pp. 351-366.
22. Li J. K-J, 2004, "Dynamics of the vascular system," World Scientific.
23. Luboz V., Hughes C., et al., 2009a. "Real-time Seldinger Technique Simulation in Complex Vascular Models". *Int. J. Comp. Assist. Rad. and Surg.*, 4(6), 589.
24. Luboz V., Blazewski R., et al., 2009b. "Real-time Guidewire Simulation in Complex Vascular Models", *Visual Computer*, 25(9), 827-834.
25. Gao L., Heath D.G., et al., 1998, "Abdominal Image Segmentation Using Three-dimensional Deformable Models". *Invest. Rad.*, 33(6), 348-355.
26. Sethian J.A., 1999, "Level Set Methods and Fast Marching Methods: Evolving Interfaces in Computational". *Geom., Fluid Mech., Comp. Vis. and Mat. Sc.*, Cambridge Univ. Press.
27. Droske M., Meyer B., et al., 2001. "An adaptive Level Set Method for Medical Image Segmentation". *Int. Conf. on Inf. Proc. in Med. Ima.*
28. Watanabe M., Kikinis R. et al., 2002. "Level Set Based Integration of Segmentation and Computational Fluid Dynamics for Flow Correction in Phase Contrast Angiography". *MICCAI*, 2489. 405 – 412.
29. Song Y., Bulpitt A.J. et al., 2008, "Efficient Semi-automatic Segmentation for Creating Patient Specific Models for Virtual Environments". *MICCAI (CVII workshop)*, 22-34.

- 1  
2  
3  
4  
5  
6  
7  
8  
9 30. Zhu S.C., Yuille A., 1996. "Region Competition: Unifying Snakes, Region Growing, and Bayes/MDL for  
10 Multiband Image Segmentation". IEEE Trans. PAMI, 18, 884-900.  
11  
12 31. Song Y., Luboz V., et al., 2011. "Segmentation of 3D vasculatures for interventional radiology simulation".  
13  
14 MMVR.  
15  
16 32. Luboz V., Zhai J., et al., 2011a. "Simulation of endovascular guidewire behaviour and experimental validation".  
17 CMBBE, online for now.  
18  
19 33. Zijdenbos A., Dawant B., et al., 1994. "Morphometric Analysis of White Matter Lesions in MR Images: Method  
20 and Validation". IEEE TMI, 13, 4.  
21  
22 34. Luboz V., Zhai J., et al., 2011b. "Guidewire and catheter behavioural simulation" MMVR.  
23  
24  
25  
26  
27  
28  
29  
30  
31  
32  
33  
34  
35  
36  
37  
38  
39  
40  
41  
42  
43  
44  
45  
46  
47  
48  
49  
50  
51  
52  
53  
54  
55  
56  
57  
58  
59  
60  
61  
62  
63  
64  
65

Mounted Phantom Omni



Stereo glasses



(b)

SimPulse

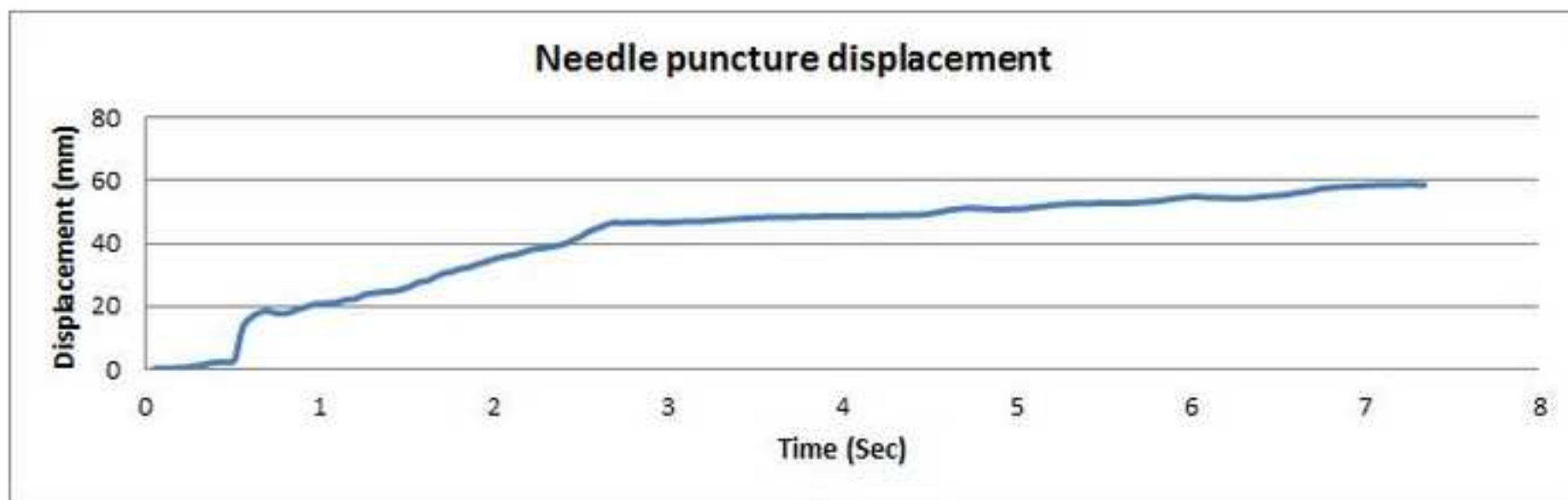


Mannequin

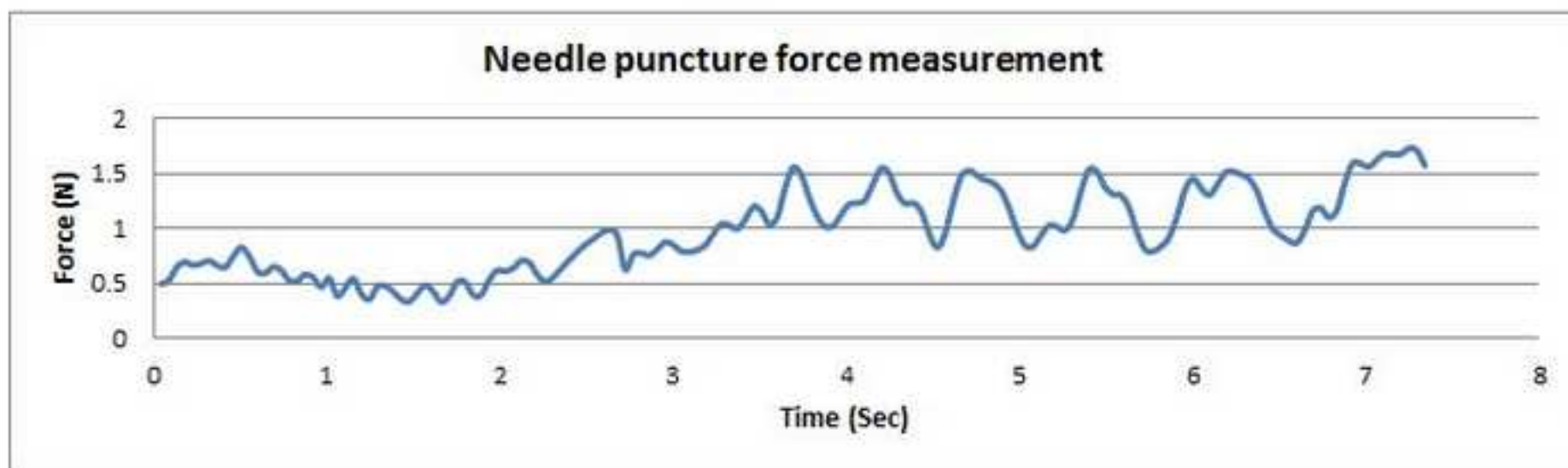
(a)

(c)

Figure 2  
[Click here to download high resolution image](#)



(a)



(b)

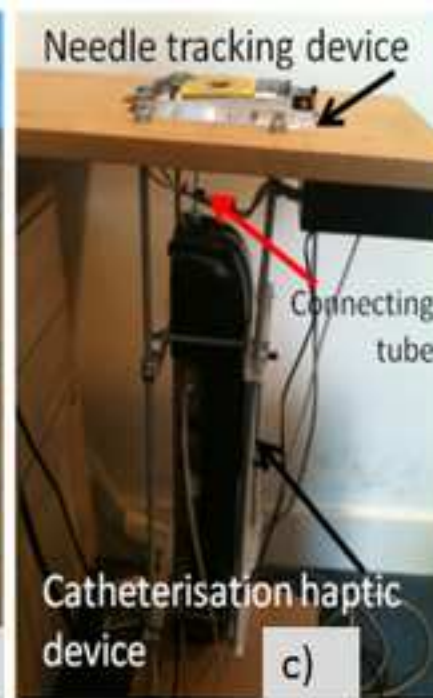
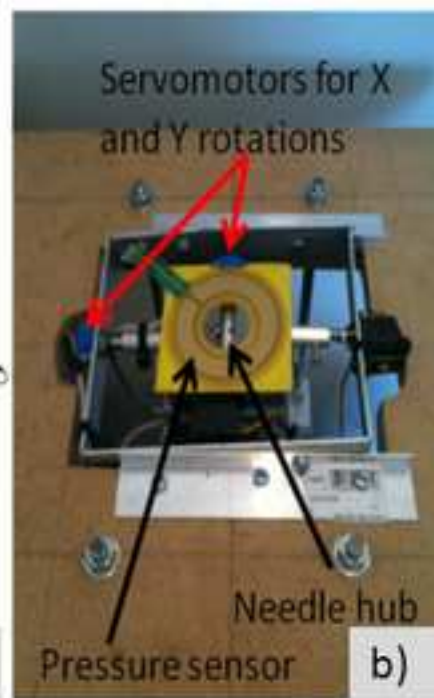
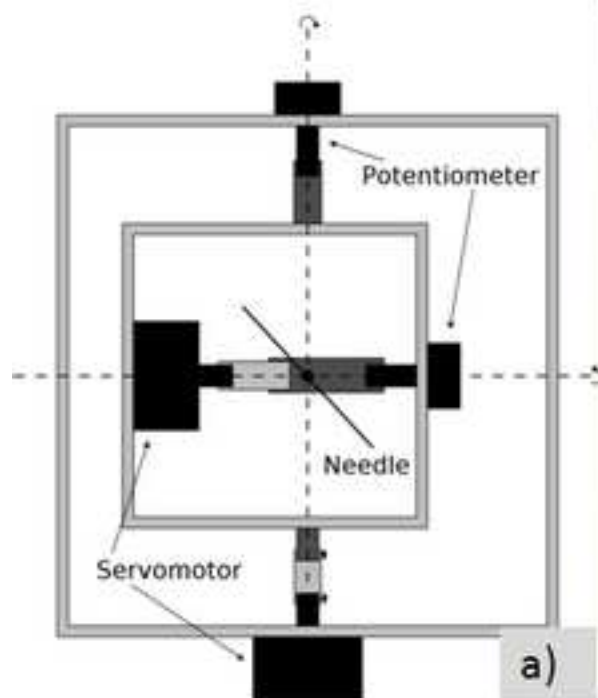




**Figure 4**  
[Click here to download high resolution image](#)

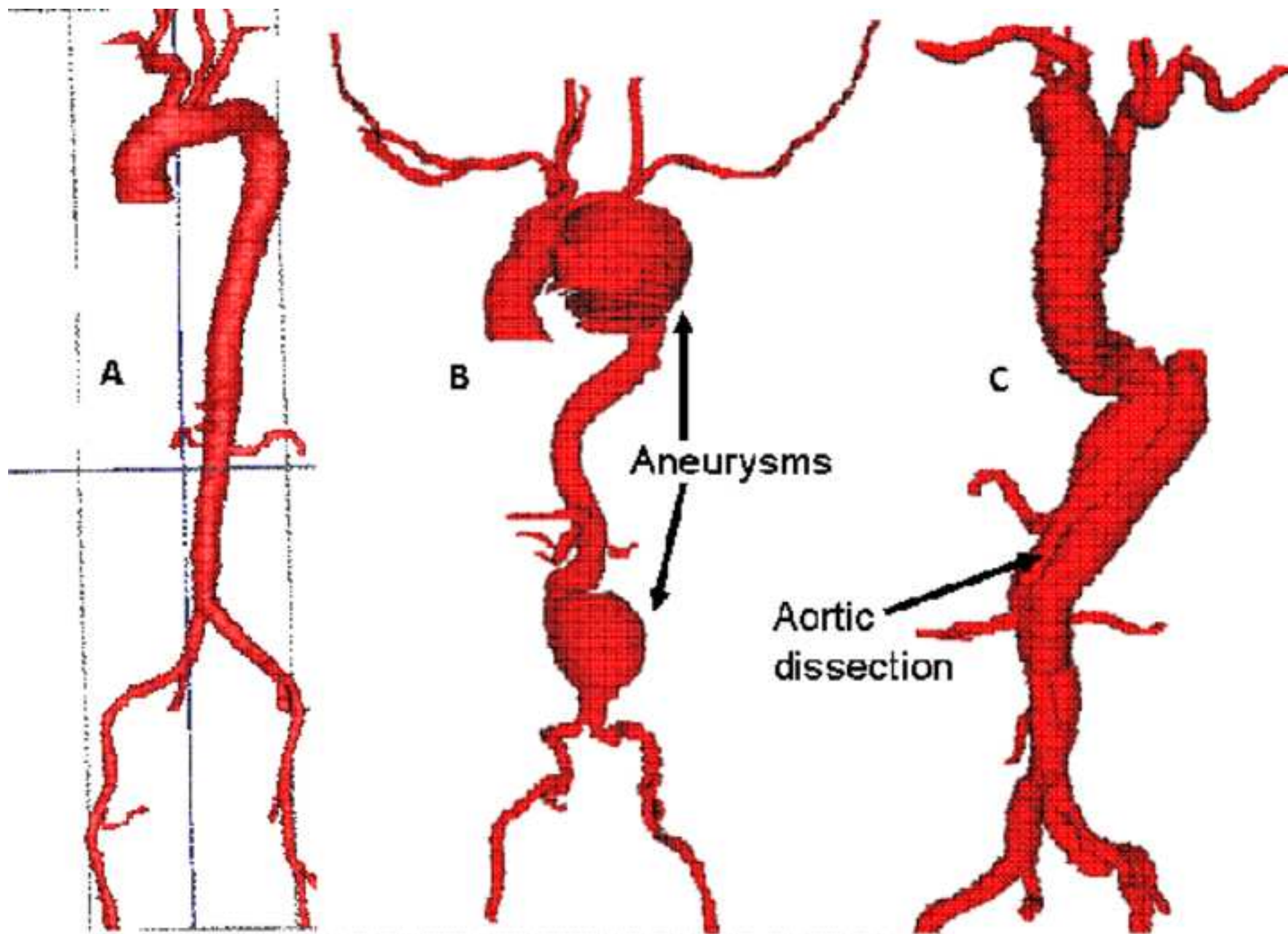
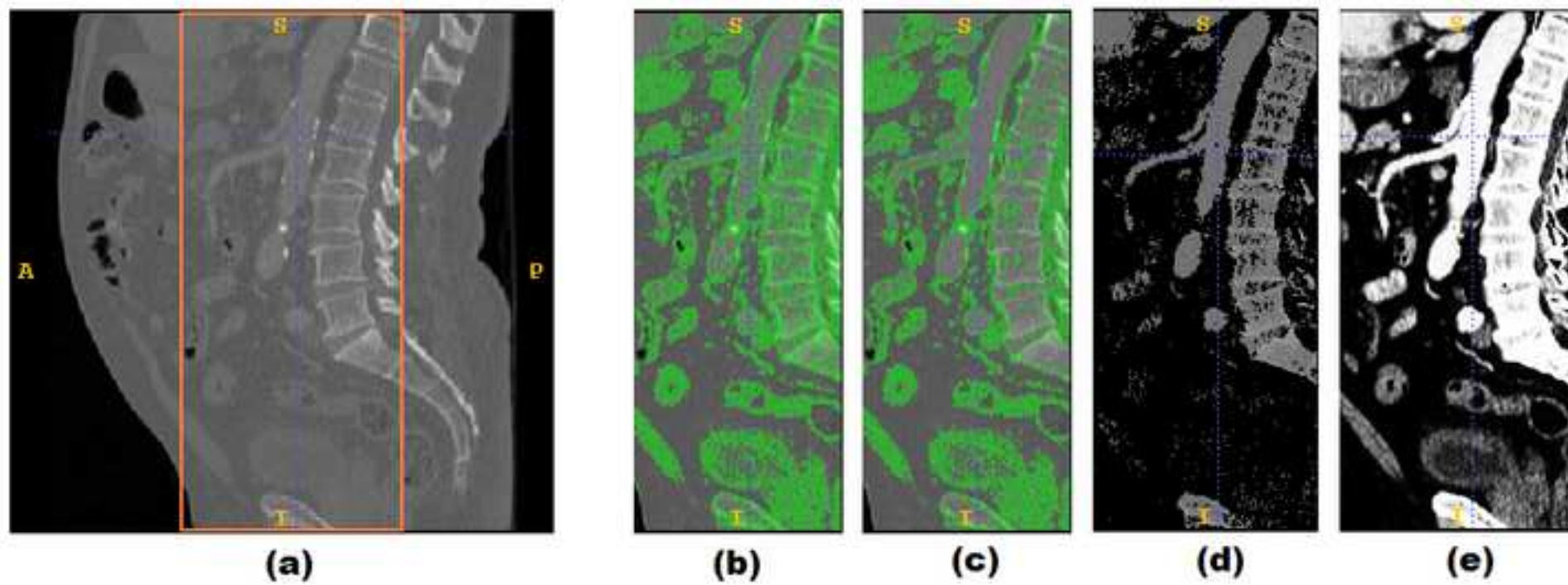




Figure 5  
[Click here to download high resolution image](#)



**Figure 6**  
[Click here to download high resolution image](#)

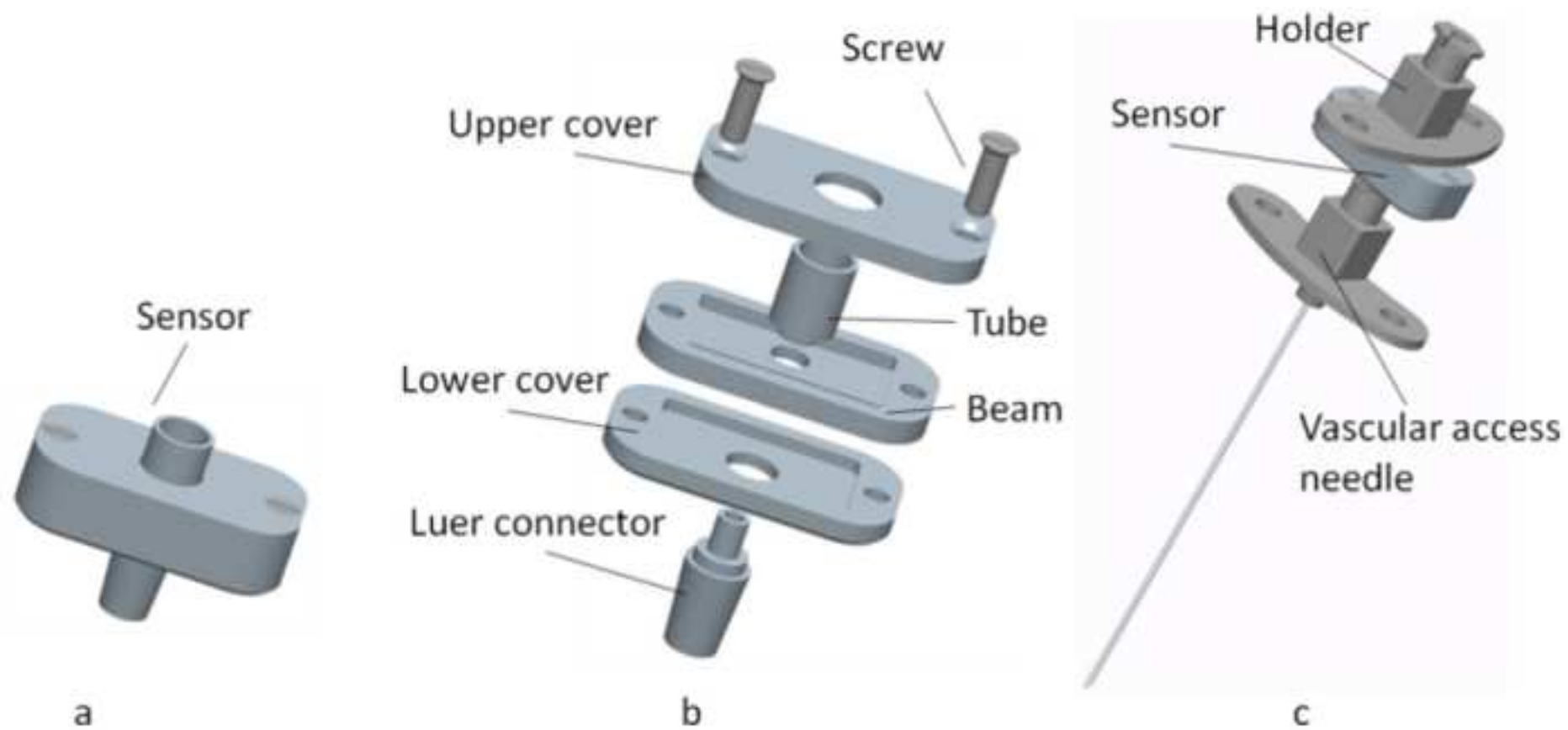


Figure 7  
[Click here to download high resolution image](#)

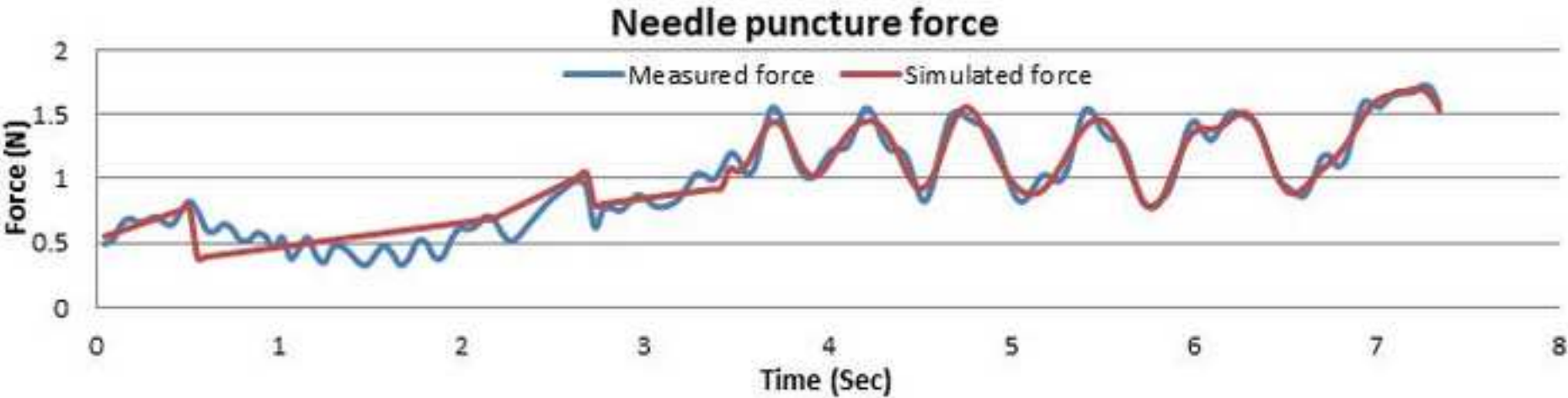
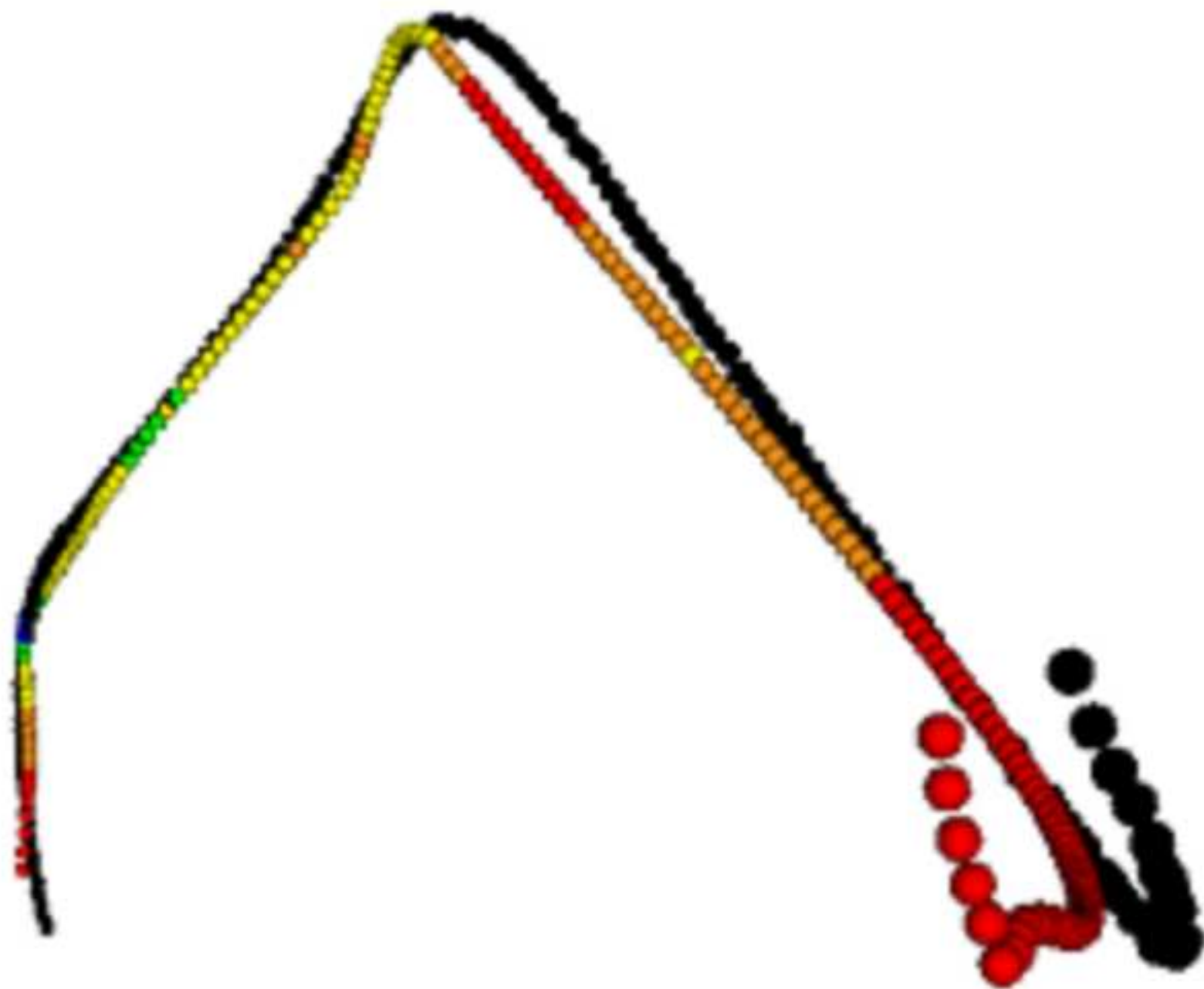


Figure 8a

[Click here to download high resolution image](#)



Figure 8b  
[Click here to download high resolution image](#)



## Supplementary Material - video

[Click here to download Supplementary Material: IMAGINE-S-2011\\_video\\_v6.avi](#)